BIOREMEDIATION JOURNAL
https://doi.org/10.1080/10889868.2025.2604133

Taylor & Francis
Taylor & Francis Group

Bioremediation potential of a multidrug-resistant *Bacillus paramycoides* BCSS17 isolated from a contaminated aquatic ecosystem

Sugitha S.[a], Abirami G.[a], Suganthi M.[b], Ashok Kumar K.[a] and Jayanthi M.[a]

[a]Department of Biotechnology, School of Life Sciences, Vels Institute of Science Technology and Advanced Studies, Chennai, Tamil Nadu, India; [b]Department of Biotechnology, Faculty of Science and Humanities, SRM Institute of Science and Technology, Kattankulathur, Tamil Nadu, India

ABSTRACT

Heavy metal pollution in aquatic environments demands effective and sustainable bioremediation solutions. This study explores the potential of *Bacillus paramycoides* BCSS17, a bacterial isolate from the contaminated waters of Buckingham Canal, for heavy metal resistance and biosorption. A total of 25 morphologically distinct bacterial isolates (BCSS01–BCSS25) were recovered, with BCSS17 exhibiting the highest Maximum Tolerable Concentration (MTC) values for lead (Pb, 2100 ppm), chromium (Cr, 1900 ppm), zinc (Zn), manganese (Mn, 1700 ppm each), and copper (Cu, 1300 ppm). Antibiotic susceptibility tests revealed multidrug resistance, and PCR amplification confirmed the presence of resistance genes *pbrA* (Pb) and *zntA* (Zn). The 16S rRNA gene was first sequenced and analyzed, revealing 100% identity with *Bacillus paramycoides*. Following identification, the sequence was submitted to the NCBI GenBank database and assigned the accession number PP989439. Growth profiling in metal-supplemented media revealed that *Bacillus paramycoides* exhibited robust growth with Pb (1.643) and Cu (1.583) at 25 h, moderate growth with Zn (1.587) and Mn (1.442), while Cr resulted in the lowest growth, with a peak OD of 1.383. Biosorption studies showed that BCSS17 exhibited the highest uptake for Pb (5.024 ± 0.57 mg/g at 100 ppm) and significant Zn uptake (4.128 ± 0.52 mg/g at 200 ppm). Bioaccumulation analysis revealed maximum accumulation of Zn (73.128 ± 0.62%) and Pb (69.435 ± 0.33%), even at higher concentrations, highlighting its strong biosorption potential. Scanning electron microscopy (SEM) analysis revealed morphological alterations in bacterial cells post-metal exposure, indicating surface-level interactions with heavy metals, while Fourier-transform infrared (FTIR) spectroscopy confirmed the involvement of functional groups such as hydroxyl (-OH), carboxyl (-COOH), amide ($-CONH_2$), and phosphate ($-PO_4^{3-}$), indicating their role in heavy metal binding. Molecular docking studies further supported these findings, revealing that Metallo beta-lactamase exhibited the strongest binding affinity with Zn (−9.6 kcal/mol), followed by Pb (−8.6 kcal/mol) and Mn (−8.3 kcal/mol), involving key interacting residues such as HIS61, HIS134, and ASP63. The novelty of this study lies in the discovery that BCSS17 exhibits exceptionally high MTC values, dual metal-resistance genes (pbrA and zntA), and superior Pb and Zn biosorption capacities—levels significantly higher than those reported for previously characterized *Bacillus* strains. These results underscore *Bacillus paramycoides* BCSS17 as a highly promising candidate for the bioremediation of heavy metal-contaminated aquatic ecosystems.

KEYWORDS

Bacillus paramycoides; bioaccumulation; bioremediation; biosorption; maximum tolerable concentration; PCR amplification

Introduction

Anthropogenic activities, such as urbanization, industrialization, and intensive agriculture, have led to widespread environmental degradation across terrestrial, atmospheric, and aquatic ecosystems. Among these, aquatic ecosystems in urban landscapes are particularly vulnerable due to the indiscriminate discharge of untreated or partially treated domestic and industrial effluents (Häder et al. 2020; Roux et al. 2024; Saqib et al. 2025). The Buckingham Canal, a man-made waterway along the eastern coast of Tamil Nadu, has undergone severe degradation due to rapid urbanization, unregulated waste disposal, and inadequate wastewater treatment (Kumar et al. 2018).

CONTACT Abirami G. drabirami.cas@gmail.com Department of Biotechnology, School of Life Sciences, Vels Institute of Science Technology and Advanced Studies, Chennai, Tamil Nadu, India.

Particularly in the Neelankarai region of Chennai, visible pollution indicators such as persistent foaming and discoloration have been observed in the canal's waters, attributed largely to the discharge of effluents from the nearby Perungudi Sewage Treatment Plant operated by Chennai Metrowater. These discharges have accelerated the accumulation of toxic heavy metals, such as iron (Fe), copper (Cu), cadmium (Cd), zinc (Zn), chromium (Cr), and lead (Pb), in the water and sediment compartments of the canal (S. Kumar et al. 2018; Kuma et al. 2020). Heavy metals are of particular concern because they are persistent, non-biodegradable, and capable of bioaccumulating in sediments and aquatic organisms. Their inputs from industrial effluents, sewage discharge, agricultural runoff, and stormwater disrupt aquatic ecosystems and pose long-term environmental and public health risks (Ahmed et al. 2022; Ghafarifarsani et al. 2024; Shahjahan et al. 2022; J. Wang 2022).

The toxic effects of heavy metals on aquatic organisms are wide-ranging and severe. Even at low concentrations, heavy metals can impair microbial communities by inhibiting essential biochemical processes such as nutrient cycling, organic matter degradation, and nitrogen fixation (Jeong et al. 2023; M. Kumar et al. 2024; Sharma et al. 2025). This leads to a decline in microbial diversity and alters the ecological functioning of the aquatic system. In higher organisms, heavy metals can bioaccumulate over time, especially in fish and benthic invertebrates. This accumulation becomes more dangerous as it biomagnifies through the food chain, affecting predators, including birds, mammals, and eventually humans (Ali and Khan 2019; Zhang et al. 2021; Banaee et al. 2024; Santhosh et al. 2024).

Microbe-based remediation is highly efficient due to the natural ability of microorganisms to survive and adapt in toxic environments. They possess specific mechanisms such as biosorption, bioaccumulation, enzymatic transformation, and metal efflux systems that enable effective removal or detoxification of heavy metals. Microbes can act quickly, require minimal energy input, and function across a wide range of environmental conditions (Podder and Majumder 2017; Deng et al. 2022). Their ease of cultivation and scalability make them suitable for both laboratory and field applications. Among various bioremediation strategies, biosorption and bioaccumulation using microorganisms have gained significant attention due to their high efficiency, cost-effectiveness, and eco-friendly nature. Biosorption involves the passive binding of metal ions onto the microbial cell surface through functional groups such as hydroxyl, carboxyl, and phosphate, whereas bioaccumulation is an active, metabolism-dependent process that transports metals into the cell (Sedlakova-Kadukova et al. 2019; A. Ullah et al. 2025; F. Ullah et al. 2025; Yushin et al. 2022). Compared to phytoremediation or chemical treatments, these microbial techniques offer faster uptake, higher specificity, and better adaptability to a wide range of environmental conditions. This dual mechanism enhances the overall metal removal efficiency, making it a potent approach for remediating heavily contaminated aquatic ecosystems.

Simultaneously, the study emphasizes exploring microbial resources, particularly heavy metal-resistant bacteria, from contaminated canal sites. A previous study by Sugitha et al. (2025) investigated the mycoremediation potential of *Curvularia lunata* isolated from the Buckingham Canal (Sugitha et al. 2025). Building on that foundation, the current study broadens the microbial scope from fungi to bacteria, offering a more comprehensive analysis of heavy metal resistance mechanisms, detailed molecular profiling, and the identification of heavy metal resistance genes (HMRGs). By exploring bacterial adaptability and genetic potential, this research offers a richer and more diverse set of discoveries, contributing significantly to the development of innovative and scalable bioremediation strategies for environmental restoration.

Method and materials

Sample collection

Water samples were collected from two distinct sites along the Buckingham Canal in the Neelankarai region of Chennai to isolate bacteria and to perform a heavy metals bioremediation study. Site 1, located upstream at 12°56′58.2″N,

80°14′54.5″E, was designated as Water Sample 1 (WS1). This site represents a relatively less disturbed section of the canal, offering a baseline for comparison. Site 2, situated downstream at 12°56′26.5″N, 80°14′48.4″E, was designated as Water Sample 2 (WS2) and is closer to known pollution sources, including effluent discharges from the nearby Perungudi Sewage Treatment Plant. Both sampling locations were selected strategically to evaluate the variation in pollution load between upstream and downstream segments. Water samples were collected in clean, acid-washed polyethylene bottles, stored at 4 °C, and transported to the laboratory for immediate analysis (Ojo et al. 2023).

Screening and isolation of bacteria from the collected water samples

Isolation of bacteria from the collected water samples was carried out to assess the microbial load and diversity present in the Buckingham Canal. Water samples from both upstream (WS1) and downstream (WS2) locations were serially diluted using sterile physiological saline (0.85% NaCl) up to 10^{-6} dilutions. From each dilution, 0.1 mL aliquots were aseptically spread onto Nutrient Agar (NA) plates for total bacteria and incubated at 37 ± 1 °C for 24–48 h (Prashanthi et al. 2021). Pure cultures were obtained using the streak plate technique. To selectively screen for heavy metal-resistant bacteria, Nutrient Agar plates were amended with 50 ppm of individual heavy metals (Zn, Pb, Mn, Cu, and Cr) and incubated at 37 °C for 24 h. Bacterial colonies that demonstrated the ability to grow under these metal-supplemented conditions were isolated and retained for further characterization.

Assessment of maximum tolerable concentration (MTC) of heavy metals for bacterial isolates

The selected heavy metal-resistant bacterial isolate was cultured on Luria–Bertani (LB) agar plates supplemented individually with different analytical-grade metal salts. The heavy metals used in this study included zinc sulfate ($ZnSO_4{\cdot}7H_2O$), copper sulfate ($CuSO_4{\cdot}5H_2O$), lead nitrate [$Pb(NO_3)_2$], manganese sulfate ($MnSO_4{\cdot}H_2O$), and potassium dichromate ($K_2Cr_2O_7$), all procured from HiMedia Laboratories, India (≥99% purity). Metal stock solutions were prepared using sterile distilled water, filter-sterilized (0.22 µm), and added to autoclaved LB agar at desired concentrations. The experiment began with 100 ppm of each metal, and plates were incubated at 37 °C for 24–48 h. Upon confirming bacterial growth, metal concentrations were increased in 100 ppm increments until no visible colony formation occurred. The Maximum Tolerable Concentration (MTC) was defined as the highest metal concentration that supported observable growth (Sevgi et al. 2010; Anwar et al. 2017; Ibrahim et al. 2021).

Antibiotic susceptibility assay of selected heavy metal-resistant bacteria

The antibiotic susceptibility of the selected heavy metal-resistant bacterial isolate was assessed using the standard Kirby-Bauer disk diffusion method on Mueller-Hinton Agar (MHA), following the guidelines outlined by the Clinical and Laboratory Standards Institute (CLSI) (Kassim et al. 2016; Humphries et al. 2021). The bacterial culture was evenly swabbed onto the surface of sterile MHA plates to create a uniform lawn of growth. Commercially available antibiotic disks (HiMedia, India), representing various classes of antibiotics, were aseptically placed on the inoculated plates using sterile forceps. The plates were then incubated at 37 °C for 18 to 24 h. After incubation, the diameters of the zones of inhibition surrounding each antibiotic disk were measured in millimeters.

Detection of heavy metal resistance genes (HMRGs) by PCR

Genomic DNA from the heavy metal-resistant isolate was extracted using the phenol-chloroform method. DNA quality was confirmed by agarose gel electrophoresis and spectrophotometry. PCR was performed to detect heavy metal resistance genes (HMRGs) using specific primers targeting genes like *chrA* (Cr), *pcoA* (Cu), *zntA* (Zn), and *pbrA* (Pb). Each 25 µL PCR reaction included template DNA, primers, dNTPs, $MgCl_2$, buffer,

and Taq polymerase. Amplification was carried out with standard thermal cycling conditions (Muhammed and Abbas 2021). PCR products were resolved on a 1.5% agarose gel and visualized under UV light. The presence of bands confirmed the occurrence of specific HMRGs in the isolate (Yang et al. 2020; Sendolo et al. 2022).

Morphological and biochemical analysis of selected heavy metal-resistant bacteria

The selected heavy metal-resistant isolate was subjected to morphological and biochemical characterization. Colony morphology was observed on nutrient agar, noting color, shape, margin, elevation, and surface texture. Gram staining revealed the cell wall type and arrangement under a light microscope. Biochemical tests included catalase, oxidase, indole, methyl red, Voges-Proskauer, citrate utilization, urease, and motility tests. These tests were performed using standard microbiological protocols. Results were compared with Bergey's Manual of Determinative Bacteriology for preliminary identification (Bergey DH & Holt JG, 2000; Hnatush et al. 2020; Dinku and Jiru 2025).

16S rRNA sequencing of selected heavy metal-resistant bacteria

The selected bacterial isolate was subjected to molecular identification through 16S rRNA gene sequencing. Genomic DNA was extracted, and the 16S rRNA gene was amplified using universal primers 27 F (5′-AGAGTTTGATCCTGGCT CAG-3′) and 1492 R (5′-TACGGYTACCTTGT TACGACTT-3′). PCR products were purified and sequenced commercially. The obtained sequence was analyzed using BLAST against the NCBI GenBank database to identify the closest phylogenetic relative. A phylogenetic tree was constructed using MEGA software to determine the evolutionary relationship (Satapute et al. 2019; Mitra et al. 2021).

Growth profile study of selected heavy metal-resistant bacteria

The growth profile of the selected heavy metal-resistant isolate was evaluated under controlled laboratory conditions. The isolate was cultured in LB broth and incubated at 37 °C with constant shaking at 150 rpm, and the pH was maintained at 5.5. Bacterial growth was monitored by measuring optical density (OD) at 600 nm at regular time intervals (every 5 h) for 24 h using a UV-Vis spectrophotometer (Sheng et al. 2008; Huang et al. 2021).

Determination of biosorption and bioaccumulation capacity of selected heavy metal-resistant bacteria

The biosorption and bioaccumulation capabilities of the isolate BCSS17 were studied to determine its efficiency in heavy metal remediation. The isolate was grown in LB broth supplemented with metal concentrations ranging from 100 ppm to 500 ppm of individual heavy metals (Zn, Cu, Pb, Cr, and Mn). The cultures were incubated at 37 °C for 24 to 48 h to allow interaction between the bacteria and the metals, enabling assessment of metal uptake efficiency. LB broth supplemented with 50 ppm of a selected heavy metal was distributed into 100 ml volumes in 250 ml conical flasks and sterilized at 15 psi for 15 min. Following sterilization, each flask was inoculated with 1 ml of freshly cultured bacterial suspension and incubated at 28 °C on a rotary shaker set at 150 rpm for 96 h, with the pH maintained at 5.5. Control flasks containing the same concentrations of heavy metals in LB broth, but without bacterial inoculation, were also included in the setup. Post-incubation, cultures were centrifuged to separate biomass from the supernatant. Residual metal concentrations in the supernatant were measured using Atomic Absorption Spectrophotometry (AAS) (Wnorowski 1991; Kim et al. 2007; Benmalek and Fardeau 2016; Li et al. 2018). The total metal removal was considered a result of biosorption (passive binding on the cell surface) and bioaccumulation (active uptake into the cell). Biosorption efficiency was calculated using Equation (1), which is widely used in microbial adsorption studies (Sugitha et al. 2025): $q\ (mg/g) = (C_0\ - C_e) \times V/M$,

Where:

- q = amount of metal biosorbed (mg/g)
- C_o = initial metal concentration (mg/L)

- C_e = equilibrium (final) metal concentration (mg/L)
- V = volume of the solution (L)
- M = dry weight of the biosorbent (g)

The elimination of heavy metals was assessed through the utilization of Equation (2) (Sugitha et al. 2025):

$$\text{Bioaccumulation/Percentage removal \%} = \frac{C_o - C_f}{C_o} \times 100$$

Where:

- C_o = initial metal concentration (mg/L)
- C_f = final metal concentration (mg/L)

Scanning Electron Microscopy (SEM) analysis

The surface morphology of the heavy metal-resistant isolate was examined using SEM to assess structural integrity and cellular alterations under metal stress. Bacterial cultures were grown in the presence and absence of selected heavy metals, harvested, and washed with phosphate-buffered saline (PBS). Samples were then fixed in 2.5% glutaraldehyde, dehydrated through a graded ethanol series, and air-dried. The dried cells were mounted on SEM stubs, sputter-coated with a thin layer of gold, and visualized under a high-resolution SEM (Titze and Genoud 2016; Khan et al. 2020). Imaging revealed distinct morphological differences between treated and untreated cells, indicating possible surface deformations, aggregation, or shrinkage due to metal exposure.

Fourier transform infrared spectroscopy (FTIR) analysis

The FTIR analysis was carried out to determine the functional groups present on the surface of the bacterial isolate BCSS17 involved in heavy metal binding. The isolate was cultured in LB broth, both in the absence (control) and presence of heavy metals (100 ppm). After 24–48 h of incubation at 37 °C, bacterial cells were harvested by centrifugation at 6000 rpm for 10 min (6,000 × g for 10 min), washed repeatedly with sterile distilled water to remove residual media, and then oven-dried at 60 °C until a fine powder was obtained. The dried biomass was finely ground with potassium bromide (KBr) and pressed into pellets. The FTIR spectra were recorded using an FTIR spectrophotometer in the range of 4000–400 cm^{-1}. Peaks were analyzed to identify shifts or changes in functional groups such as carboxyl, hydroxyl, amine, and phosphate, indicating their role in heavy metal interaction and biosorption (Nandiyanto et al. 2019; Sugitha et al. 2025).

Molecular docking analysis of selected heavy metal-resistant bacteria

Molecular docking between heavy metals and selected target proteins was performed using AutoDock Vina (https://autodock.scripps.edu) (Trott and Olson 2010; Eberhardt et al. 2021). Before docking, the protein structures were prepared by converting them into macromolecules and saved in PDBQT format. Default docking parameters were used, except for the grid box, which was manually defined around the protein's crystal structure to specify the binding site. Docking simulations generated multiple binding conformations, which were evaluated based on their binding affinities (ΔG). The best-docked poses were selected by identifying those with the lowest binding energy. Interaction analysis between heavy metals and protein residues, such as hydrogen bonds, van der Waals forces, alkyl, π-alkyl, and halogen interactions, was performed using BIOVIA Discovery Studio Visualizer 2.5 (http://3dsbiovia.com/products/)(Ayodele et al. 2023). Further confirmation and visualization of molecular interactions were achieved using both DS Visualizer 2.5 and PyMOL Molecular Graphics System 2.0(Seeliger and de Groot 2010; Chaudhari and Li 2015; El Khoury et al. 2023).

The two-dimensional (2D) structures of selected heavy metal compounds (PubChem IDs: 14806, 517277, 14829, 14801, and 24459) were retrieved in Spatial Data File (SDF) format from the NCBI PubChem database (https://pubchem.ncbi.nlm.nih.gov/) and converted into PDB format using PyMol and MolView (MolView.org) (Kim et al. 2016, 2023; Sehnal et al. 2021; Y. Wang et al. 2010). Table 1 presents the proteins with PDB IDs 6KNS and 3I9Z were selected

Table 1. Crystallographic data of target proteins.

Target Proteins	Experimental Data
PDB ID: 6KNS (Metallo beta lactamse) 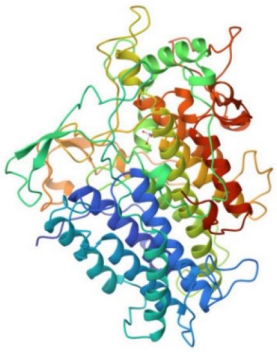	• Method: X-RAY DIFFRACTION • Resolution: 2.15 Å • R-Value Free: 0.202 • R-Value Work: 0.168 • R-Value Observed: 0.170
PDB ID: 3I9Z (Metallochaperone) 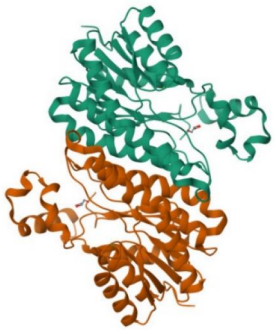	• Method: X-RAY DIFFRACTION • Resolution: 1.90 Å • R-Value Free: 0.265 • R-Value Work: 0.191 • R-Value Observed: 0.191
GeneBank: QDZ76690.1(Metallothionein) 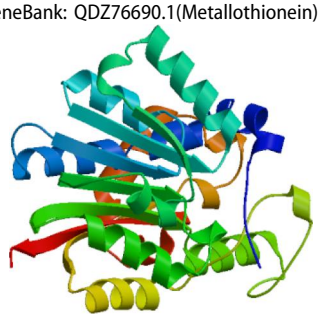	• Method: X-RAY DIFFRACTION • Resolution: 1.60 Å • Seq Similarity: 0.26 • Coverage: 0.67

based on their functional roles in metal resistance and their high sequence similarity to proteins in the isolate BCSS17, confirmed through BLAST analysis. These structures were available in the PDB and provided suitable templates for molecular studies (Burley et al. 2021). The third protein, QDZ76690.1, had no available structure and was modeled *via* homology modeling using its GenBank sequence (Sayers et al. 2022, 2024).

Statistical analysis

All experimental data were statistically analyzed using GraphPad Prism (version 9) software. Results were expressed as mean ± standard deviation (SD) from at least three independent replicates. Statistical significance between groups was determined using one-way and two-way ANOVA, followed by Tukey's post hoc test. A p-value < 0.05 was considered statistically significant. Graphs were generated to visualize variations in the growth profile study, heavy metal uptake, and bioaccumulation values. The software facilitated a clear and precise representation of data trends and variability (Berkman et al. 2019; Sugitha et al. 2025).

Results

Screening and isolation of bacteria from the collected water samples

A total of 25 morphologically distinct bacterial colonies were isolated based on differences in

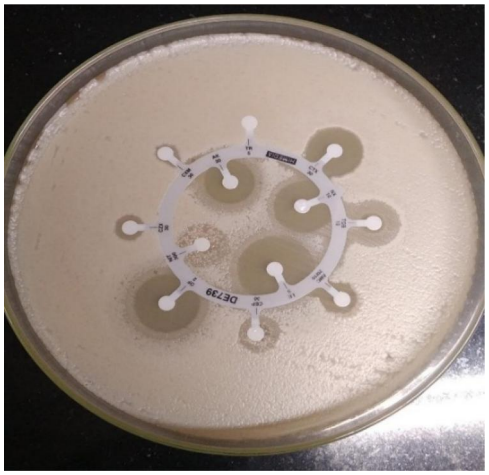

Figure 1. Antibiotic susceptibility assay for the selected isolate BCSS17.

Table 2. Antibiotic susceptibility test for the selected heavy metal-resistant isolate BCSS17.

Antibiotics	BCSS17
Cephalothin (CEP) 30 mcg	R
Ceftizoxime (CZX) 30 mcg	R
Cefuroxime (CXM) 30 mcg	R
Cefotaxime (CTX) 30 mcg	S
Amoxiclav (AMC) 20/10 mcg	R
Norfloxacin (NX) 10 mcg	S
Ofloxacin OF (OF) 2 mcg	S
Levofloxacin (LE) 5 mcg	S
Nitrofurantoin (NIT) 300 mcg	R
Trimethoprim (TR) 5 mcg	R
Amikacin (AK) 30 mcg	S
Tobramycin (TOB) 10 mcg	R

colony shape, size, color, elevation, and margin. These isolates, designated as BCSS01 to BCSS25, were selected for further characterization and screening to assess their tolerance to heavy metals. The result shows that Sample 1 had the highest bacterial load of 3.2×10^5 CFU/mL, while Water Sample 2 recorded 2.1×10^5 CFU/mL. The relatively high colony count reflects the canal's organic and inorganic pollutant load, indicating active microbial adaptation to the contaminated environment.

MTC of heavy metals for bacterial isolates

The MTC of five heavy metals was assessed across all 25 bacterial isolates, with concentrations ranging from 100 ppm to 2100 ppm. All isolates exhibited varying degrees of resistance to the tested metals, indicating a strong adaptive response to the contaminated canal environment.

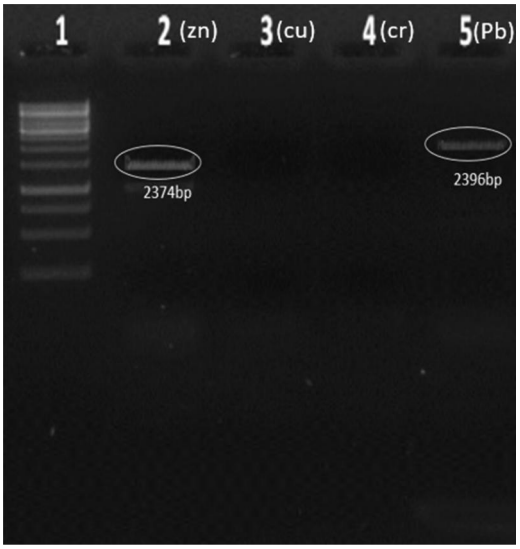

Figure 2. PCR amplification of HMRGs.

Among them, BCSS17 stood out by displaying the highest MTC values for multiple heavy metals, highlighting their superior resistance potential. While BCSS17 was selected for continued analysis in the present study due to its comparable and consistent tolerance, making it a promising candidate for future bioremediation applications. The BCSS17 isolate exhibited maximum tolerable concentrations of 2100 ppm for Pb, 1900 ppm for Cr, 1700 ppm for both Zn and Mn, and 1300 ppm for Cu, respectively.

Antibiotic susceptibility assay for the selected heavy metal-resistant isolate BCSS17

The antibiotic susceptibility profile of BCSS17 was evaluated using the Kirby-Bauer disk diffusion method against a panel of commonly used antibiotics. The isolate exhibited resistance (R) to Cephalothin (CEP), Ceftizoxime (CZX), Cefuroxime (CXM), Amoxiclav (AMC), Nitrofurantoin (NIT), Trimethoprim (TR), and Tobramycin (TOB). In contrast, it was found to be sensitive (S) to Cefotaxime (CTX), Norfloxacin (NX), Ofloxacin (OF), Levofloxacin (LE), and Amikacin (AK) (Figure 1) (Table 2). This mixed susceptibility pattern highlights the presence of multidrug resistance traits, which may be linked to the isolate's environmental adaptation to contaminated and antibiotic-exposed aquatic ecosystems.

PCR amplification of HMRGs in heavy metal-resistant isolate BCSS17

Gene amplification analysis revealed that the *zntA*, *pcoA*, *pbrA*, and *chrA* genes produced amplicons of approximately 2374, 1791, 2396, and 520 bp, respectively. Notably, BCSS17 exhibited successful amplification for both the *pbrA* and *zntA* genes, indicating its potential for resistance to lead and zinc, respectively (Figure 2).

Morphological and biochemical analysis of heavy metal-resistant isolate BCSS17

The isolate BCSS17 was identified as a rod-shaped and Gram-positive bacterium. Biochemical characterization showed that it was positive for catalase, nitrate reductase, citrate utilization, ammonia production, casein hydrolysis, methyl red (MR), and Voges-Proskauer (VP) tests. However, it tested negative for oxidase, urease, indole production, indole-3-acetic acid (IAA) production, and starch hydrolysis (refer to Table 3). These results indicate that BCSS17 possesses traits associated with plant growth promotion and organic matter degradation.

Table 3. Biochemical analysis of heavy metal-resistant isolate BCSS17.

Tests	BCSS17
Oxidase test	–
Catalase test	+
Nitrate reductase test	+
Urease test	–
Indole production test	–
Citrate utilization test	+
Ammonia production test	+
IAA production test	–
Casein hydrolysis test	+
Starch hydrolysis test	-
Methyl red test	+
VP (Voges Proskauer) test	+

16S rRNA sequencing of heavy metal-resistant isolate BCSS17

The selected heavy metal-resistant bacterial isolate BCSS17 was subjected to 16S rRNA gene sequencing, followed by NCBI BLAST analysis and phylogenetic tree construction for molecular characterization. BLAST results confirmed that BCSS17 shares 100% identity and 100% query coverage with *Bacillus paramycoides*. As illustrated in Figure 3, the isolate exhibited 96% sequence similarity with *Bacillus paramycoides*, highlighting a close phylogenetic relationship. Followed by 16S rRNA gene sequence of *Bacillus paramycoides* strain BCSS17 has been successfully submitted to GenBank and is available under the accession number PP989439.

Growth profile study of Bacillus paramycoides

The growth profile of the bacterial isolate was monitored over 30 h in the presence of various heavy metals (Zn, Cu, Mn, Pb, and Cr) and compared with a control. At 0 h, all samples showed similar optical density values, indicating a uniform initial bacterial load. In the presence of Zn and Mn, bacterial growth increased progressively, peaking at 25 h with OD values of 1.587 and 1.312, respectively, before slightly declining. Notably, Pb supported substantial growth, with OD values rising consistently and peaking at

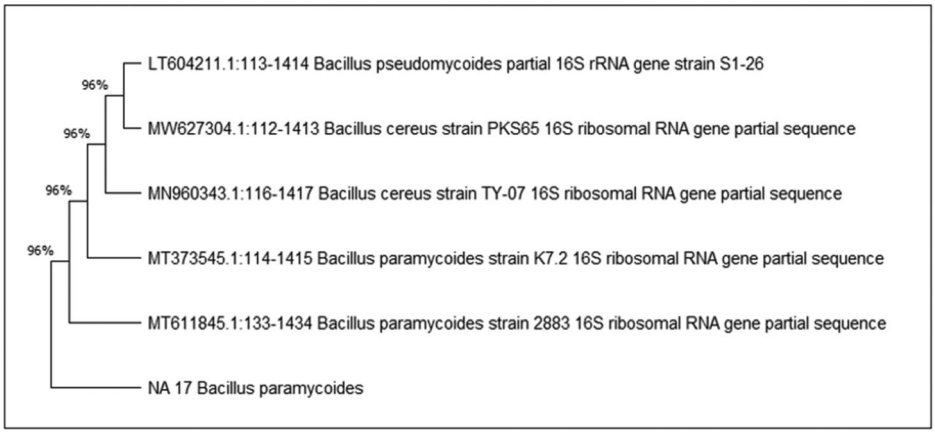

Figure 3. Phylogenetic tree of heavy metal-resistant isolate BCSS17.

1.643 at 25 h, indicating higher tolerance. Cu and Cr showed comparatively lower growth, with Cr in particular exhibiting the least supportive conditions for bacterial proliferation, reaching only 1.383 OD at 25 h before declining (refer to Table 4 and Figure 4).

These results suggest that the isolate shows significant tolerance to Pb, Zn, and Mn, while growth was inhibited to a greater extent in the presence of Cu and Cr. A two-way ANOVA revealed significant effects of both heavy metal type and incubation duration on the growth of *Bacillus paramycoides* ($p < 0.001$). Post-hoc Tukey's test showed that copper and chromium significantly suppressed growth compared to control across most time points ($p < 0.05$).

Lead and zinc allowed near-normal growth, while manganese showed moderate stimulation until 20 h, after which growth declined.

Table 4. Growth profile of *Bacillus paramycoides* in the presence of heavy metals.

Duration (hrs)	Control	Zn	Cu	Mn	Pb	Cr
0	0.733	0.732	0.723	0.743	0.742	0.763
5	1.168	0.924	0.732	0.976	0.894	0.742
10	1.256	1.198	0.885	1.198	0.965	0.855
15	1.387	1.213	0.996	1.235	1.353	0.996
20	1.654	1.267	1.212	1.442	1.542	1.312
25	1.832	1.587	1.583	1.312	1.643	1.383
30	1.854	1.221	1.153	1.176	1.622	1.183

Biosorption and bioaccumulation study by Bacillus paramycoides

The heavy metal uptake potential of *Bacillus paramycoides* was evaluated at different concentrations (100–500 ppm) for five metals: Zn, Cu, Mn, Pb, and Cr. Among these, BCSS17 exhibited the highest uptake for Pb, with a maximum of 5.024 ± 0.57 mg/g at 100 ppm and sustained efficient uptake at higher concentrations, including 3.435 ± 0.33 mg/g at 400 ppm. Uptake of Zn was also notable, reaching 4.128 ± 0.52 mg/g at 200 ppm and 3.321 ± 0.52 mg/g at 300 ppm. Moderate uptake was recorded for Mn and Cr, with peak values of 3.144 ± 0.52 mg/g and 3.127 ± 0.34 mg/g, respectively. Copper uptake was relatively lower, decreasing to 0.723 ± 0.13 mg/g at 400 ppm (refer to Table 5 and Figure 5). Overall, the data indicate that BCSS17 is highly efficient in biosorbing Pb and Zn, suggesting strong potential for use in the bioremediation of heavy metal-contaminated environments. One-way ANOVA showed a standard deviation ($n = 3$) and statistically significant difference in heavy metal uptake efficiency among the tested metals ($p = 0.028$). Tukey's post-hoc test revealed that Pb uptake was significantly higher than Cr and Cu ($p < 0.05$). No significant differences were found among the other metal pairs.

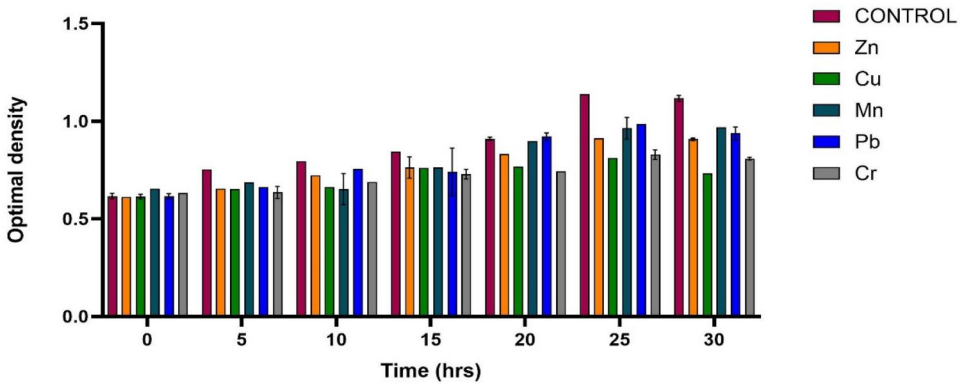

Figure 4. Growth profile of *Bacillus paramycoides* in the presence of heavy metals.

Table 5. Biosorption (mg/g) of *Bacillus paramycoides* at varying metal concentrations.

Heavy Metals	100 ppm	200 ppm	300 ppm	400 ppm	500 ppm
Zn	3.89 ± 0.52	4.128 ± 0.52	3.321 ± 0.52	2.232 ± 0.55	1.247 ± 0.32
Cu	2.651 ± 0.24	2.239 ± 0.42	1.126 ± 0.51	0.723 ± 0.13	0.828 ± 0.26
Mn	2.764 ± 0.42	3.144 ± 0.52	2.321 ± 0.11	1.411 ± 0.23	1.131 ± 0.42
Pb	5.024 ± 0.57	4.223 ± 0.32	2.765 ± 0.82	3.435 ± 0.33	2.646 ± 0.43
Cr	3.127 ± 0.34	2.131 ± 0.43	2.789 ± 0.87	1.242 ± 0.22	0.367 ± 0.84

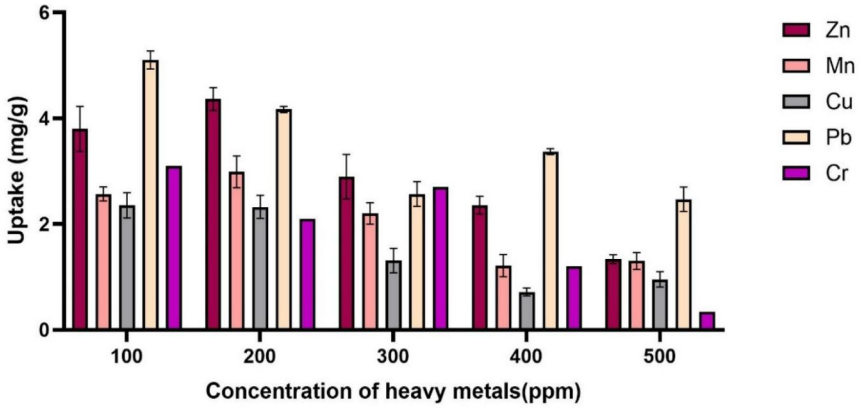

Figure 5. Biosorption of *Bacillus paramycoides* at varying metal concentrations.

Table 6. Bioaccumulation efficiency (%) of *Bacillus paramycoides* at varying metal concentrations.

Heavy Metals	100 ppm	200 ppm	300 ppm	400 ppm	500 ppm
Zn	72.625 ± 0.53	73.128 ± 0.62	63.321 ± 0.32	68.232 ± 0.52	50.247 ± 0.12
Cu	40.651 ± 0.29	41.239 ± 0.52	36.122 ± 0.26	30.733 ± 0.53	28.228 ± 0.24
Mn	46.764 ± 0.42	32.144 ± 0.62	22.311 ± 0.19	14.411 ± 0.23	21.131 ± 0.42
Pb	66.024 ± 0.67	64.223 ± 0.32	53.765 ± 0.82	69.435 ± 0.33	59.546 ± 0.34
Cr	47.127 ± 0.64	43.131 ± 0.23	46.789 ± 0.87	31.242 ± 0.24	30.367 ± 0.84

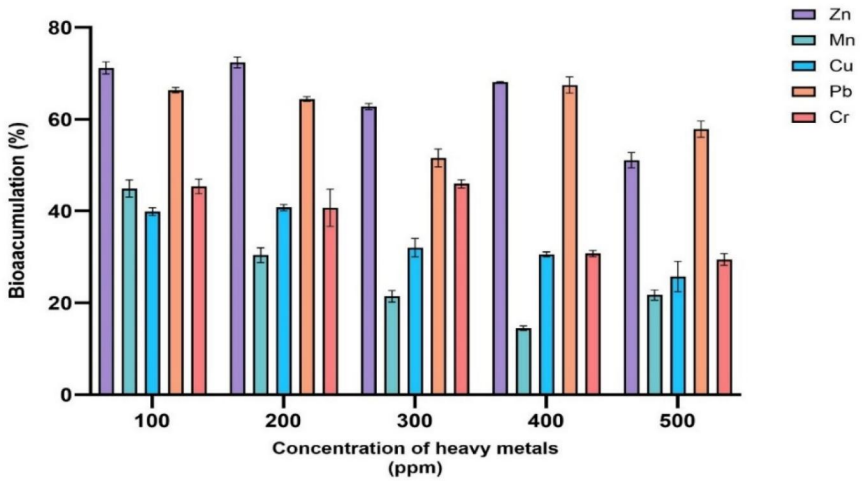

Figure 6. Bioaccumulation efficiency of *Bacillus paramycoides* at varying metal concentrations.

The bioaccumulation efficiency of *Bacillus paramycoides* was assessed at varying concentrations (100–500 ppm). Among all five heavy metals, Zn showed the highest accumulation across all concentrations, with a peak of 73.128 ± 0.62% at 200 ppm and a notable retention of 50.247 ± 0.12% at 500 ppm, indicating strong metal-binding capacity. Pb also exhibited high accumulation, reaching 69.435 ± 0.33% at 400 ppm, suggesting that BCSS17 is particularly effective in Pb biosequestration even at higher concentrations. Moderate bioaccumulation was recorded for Cr, with values ranging from 47.127 ± 0.64% at 100 ppm to 30.367 ± 0.84% at 500 ppm. In contrast, Cu and Mn showed comparatively lower bioaccumulation, especially at higher concentrations, with Mn dropping to 14.411 ± 0.23% at 400 ppm (refer to Table 6 and Figure 6). Overall, the statistical analysis indicated standard deviation ($n = 3$) and highly significant differences among treatments ($F = 18.70$, $p < 0.05$). Tukey's post-hoc test further revealed that Zn and Pb exhibited significantly higher uptake at moderate concentrations (200–

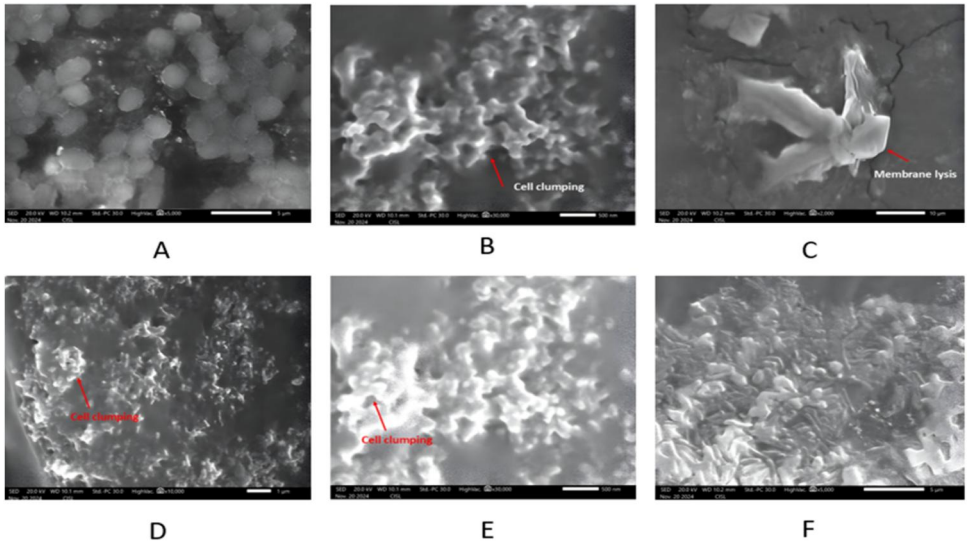

Figure 7. SEM analysis of *Bacillus paramycoides* in the presence of heavy metals - (A) control, (B) Zn, (C) Pb, (D) Mn, (E) Cu, and (F) Cr.

400 ppm), whereas the bioaccumulation efficiency for Cu, Mn, and Cr declined sharply at higher concentrations.

SEM analysis of Bacillus paramycoides *in the presence of heavy metals*

The morphological alterations in bacterial cells upon exposure to heavy metals were analyzed using Scanning Electron Microscopy. The control sample displayed healthy, intact cells with smooth surfaces and uniform shape, indicating normal morphology in the absence of metal stress. In contrast, significant structural changes were observed in the metal-treated cells. Zn-treated cells exhibited prominent cell clumping, suggesting cellular aggregation possibly due to stress-induced surface charge modifications. Pb exposure caused severe membrane lysis and disintegration, indicative of high toxicity and disruption of membrane integrity. Similarly, Mn and Cu treatments resulted in cell clumping, although the extent varied, implying moderate cellular stress. Cr-treated cells showed rough and disrupted surfaces, pointing to oxidative damage and loss of cellular architecture (Figure 7). These observations collectively suggest that heavy metal exposure induces notable morphological stress in *Bacillus paramycoides*, with Pb and Cr causing the most pronounced cellular damage.

FTIR analysis of Bacillus paramycoides *in the presence of heavy metals*

The FTIR spectrum of *Bacillus paramycoides* treated with Zn showed moderate spectral changes, indicating surface-level biosorption. The broad O–H/N–H stretching band, typically located within the 3200–3400 cm^{-1} region, shifted slightly to 3282.18 cm^{-1}, reflecting minor interactions between Zn and hydroxyl or amine groups. The Amide I (1600–1700 cm^{-1}) and Amide II (1500–1560 cm^{-1}) bands appeared at 1628.14 and 1533.90 cm^{-1}, respectively, suggesting moderate involvement of protein functional groups. A prominent peak at 1226.70 cm^{-1}, falling within the C–N/P = O/C–O stretching range (1200–1260 cm^{-1}), alongside a shift at 1042.90 cm^{-1} in the C–O/P–O region (1020–1080 cm^{-1}), indicates interaction with polysaccharide or phosphate groups. The absence of metal–O bands in the 500–650 cm^{-1} region suggests weaker or less direct coordination compared to Cu or Cr (Table 7; Figure 8B). Overall, Zn binds mainly *via* surface polysaccharides and proteins, causing minimal structural alterations.

The Pb-treated biomass exhibited distinctive spectral features indicative of strong biosorption. A clear peak emerged at 1724.02 cm^{-1}, corresponding to C=O stretching (1700–1750 cm^{-1}), suggesting Pb binding with carbonyl-containing groups such as carboxyls or esters (Figure 8C).

Table 7. FTIR analysis of *Bacillus paramycoides* in the presence of heavy metals.

Control	Zn	Pb	Mn	Cu	Cr	Functional Group
3282.04	3282.18	3280.61	3275.11	3275.26	3275.26	O–H / N–H stretching
2923.73	2929.3	2928.15	2926.76	2927.70	2927.70	C–H (aliphatic)
—	—	1724.02	1724.06	—	—	C = O (carbonyl)
1631.07	1628.14	1633.75	1633.90	1626.81	1626.81	Amide I / COO^-
1546.13	1533.9	1549.61	1539.06	—	1548.94	Amide II
1449.99	1393.4	1399.35	1399.21	1398.46	1398.46	COO^- symmetric stretch
1401.22	—	—	—	—	1451.25	Possibly CH_2 / C–C / deformation
1233.68	1226.7	—	1230.27	—	—	C–N / P = O / C–O
1045.95	1042.9	—	1055.32	1071.13	1071.13	C–O / P–O
—	—	979.08	—	932.26	932.26	P–O or C–O
469.93	—	530.09, 572.26	514.56	521.25, 617.57	521.25, 617.57	Metal–O

The O–H/N–H stretching band (3200–3400 cm^{-1}) shifted from 3282.04 to 3280.61 cm^{-1}, showing a redshift associated with hydrogen bonding or metal ion complexation. The Amide I and Amide II bands intensified and shifted to 1633.75 and 1549.61 cm^{-1}, respectively, indicating strong interaction with protein backbones. The symmetric COO^- stretch, typically found in the 1380–1420 cm^{-1} region, was observed at 1399.35 cm^{-1}, confirming carboxyl involvement. Additionally, a unique peak at 979.08 cm^{-1}, within the P–O/C–O region (900–1000 cm^{-1}), suggests Pb interaction with phosphate or hydroxyl groups. Collectively, these spectral shifts indicate that carboxyl, hydroxyl, amino, and phosphate groups all contribute to Pb biosorption, mediated through both protein and polysaccharide components.

The Mn-treated cells showed a distinct band at 1724.06 cm^{-1}, corresponding to C=O (carbonyl) stretching typically observed in the 1700–1750 cm^{-1} region, indicating Mn interaction with carbonyl-containing groups (Figure 8D). The broad O–H/N–H stretching band, usually found around 3200–3400 cm^{-1}, redshifted from 3282.04 to 3275.11 cm^{-1}, confirming metal coordination with hydroxyl or amine groups. Amide I and II bands, characteristic of protein vibrations at 1600–1700 cm^{-1} and 1500–1560 cm^{-1}, appeared at 1633.90 and 1539.06 cm^{-1}, suggesting protein–metal interactions. The peak at 1230.27 cm^{-1} (within the 1220–1260 cm^{-1} range), associated with C–N or P = O stretching, and a shift at 1055.32 cm^{-1} (typical for C–O/P–O stretching at 1020–1080 cm^{-1}) indicate involvement of polysaccharide and phosphate groups in Mn binding. These results show that Mn interacts with the biomass primarily through carboxyl, phosphate, and protein-associated groups, similar to Pb but with less pronounced protein deformation.

For Cu treatment, the absence of a 1724 cm^{-1} carbonyl band indicates minimal involvement of C=O groups. However, strong shifts at 1071.13 cm^{-1} (within the phosphate C–O/P–O region of 1050–1100 cm^{-1}) and in the low-frequency metal–O region (520–650 cm^{-1}) confirm Cu interaction with phosphate and sugar-like residues. The downshift of the Amide I band to 1626.81 cm^{-1} and disappearance of Amide II (1500–1560 cm^{-1}) imply Cu-induced protein structural modification. The broad O–H/N–H band also redshifted to 3275.26 cm^{-1}, again indicating hydrogen bonding or coordination. These results suggest that Cu predominantly binds through phosphate groups and causes more significant protein alteration than Pb or Mn.

The Cr spectrum resembled that of Cu, with shared peaks at 1071.13, 521.25, and 617.57 cm^{-1}, consistent with phosphate and metal–oxygen coordination. A unique peak at 1451.25 cm^{-1} (within the CH_2/C–C deformation range of 1400–1470 cm^{-1}) indicates Cr-induced structural modification of cell wall components. Amide I and II bands remained at 1626.81 and 1548.94 cm^{-1}, suggesting moderate protein involvement without major disruption. The strong band at 932.26 cm^{-1} (typical for P–O stretching around 900–950 cm^{-1}) supports the participation of phosphate groups. The redshift in the O–H/N–H band to 3275.26 cm^{-1} and stable COO^- band at 1398.46 cm^{-1} reinforce the role of hydroxyl, carboxyl, and phosphate groups in Cr coordination, indicating a binding behavior that is distinct from Pb and Mn.

Molecular docking studies of Bacillus paramycoides *proteins with various heavy metals*

The molecular docking analysis of *Bacillus paramycoides* proteins with various heavy metals

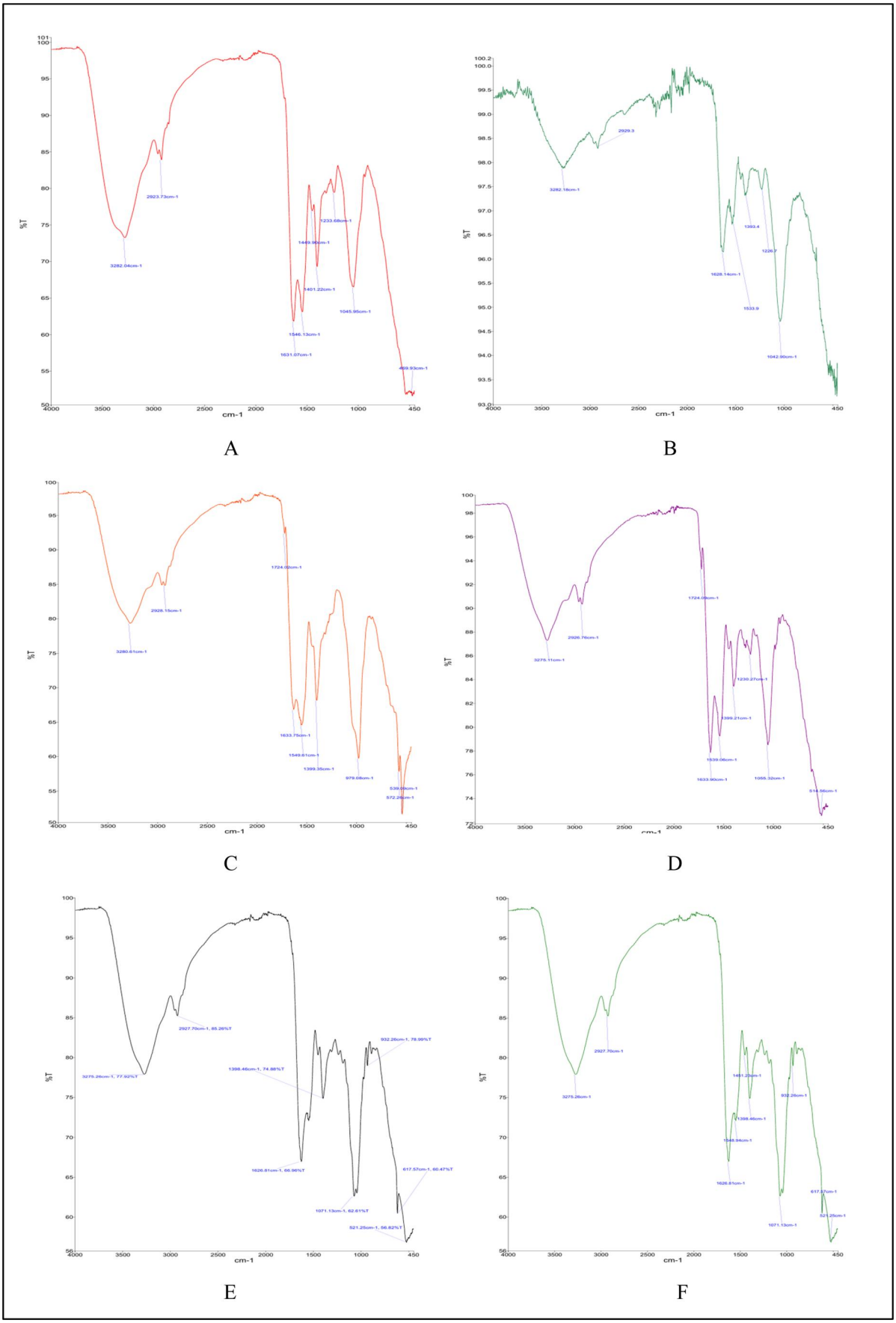

Figure 8. FTIR analysis of *Bacillus paramycoides* in the presence of heavy metals - (A)control, (B) Zn, (C) Pb, (D) Mn, (E) Cu, and (F) Cr.

Table 8. The protein interaction residues and H-bond distance.

Proteins	Heavy metals	Binding energy (kcal/mol)	Interacting residues
Metallo beta lactamse	Zinc Oxide	−9.6	HIS A:61, HIS A:62, HIS A:134, HIS A:189, HIS A:211, ASN A:177, ASP A:63, ALA A:187
	Chromium Oxide	−4.3	HIS A:214, PHE A:215, PHE A:178, PRO A:213, PHE A:12, ASN A:177, ASP A:63, GLY A:11, HIS A:211, HIS A:61
	Copper Oxide	−6.5	HIS A:59, HIS A:61, ASP A:63, HIS A:134, ASP A:155, HIS A:189, ASN A:177, PRO A:213, HIS A:214
	Manganese Oxide	−8.3	ILE A:65, ILE A:68, LYS A:102
	Lead Chloride	−8.6	ASN A:177, HIS A:189, HIS A:211, ASP A:63, ASP A:155, HIS A:61
Metallochaperone	Zinc Oxide	−8.3	ASP A:43, HIS A:34, LYS A:41
	Chromium Oxide	−5.4	ASP A:58, ALA A:57, ILE A:70, VAL A:53, LYS A:54
	Copper Oxide	−6.5	ASP A:58, ALA A:57, ILE A:70, VAL A:53, LYS A:54
	Manganese Oxide	−8.0	VAL A:53, LYS A:54, ALA A:57, VAL A:67, ILE A:70
	Lead Chloride	−6.7	GLU A:2, LYS A:4, ALA A:48, SER A:52, VAL A:53, ARG A:73
Metallothionein	Zinc Oxide	−8.8	LYS A:4, TRP A:21, SER A:19, LEU A:17
	Chromium Oxide	−7.9	TRP A:21, LYS A:4, LEU A:17, ILE A:6, LYS A:8, VAL A:20Top of Form Bottom of Form
	Copper Oxide	−6.0	THR A:10, GLU A:12, LYS A:29, LYS A:30
	Manganese Oxide	−8.8	CYS A:11, HIS A:13, LEU A:18, LYS A:29, TYR A:31
	Lead Chloride	−7.1	CYS A:11, HIS A:13, GLU A:12, LYS A:30, GLY A:28

revealed notable interactions, indicating the bacterium's potential for heavy metal bioremediation. Metallo beta-lactamase showed the strongest binding with Zinc oxide (−9.6 kcal/mol), involving key residues like HIS A:61, HIS A:62, HIS A:134, HIS A:189, HIS A:211, ASN A:177, ASP A:63, and ALA A:187, suggesting a high affinity for Zinc oxide. Metallochaperone also showed significant affinity for Zinc and Manganese oxides (−8.3 and −8.0 kcal/mol), with residues ASP A:43, HIS A:34, and LYS A:41 involved. Metallothionein interacted notably with Zinc and Manganese oxides (−8.8 kcal/mol), highlighting residues like CYS A:11 and TRP A:21(refer to Table 8, Figure 9, Figure 10, and Figure 11). The moderate interactions observed with chromium and copper oxides further suggest that *B. paramycoides* is a promising candidate for multi-metal detoxification.

Discussion

The findings of this study underscore the significant microbial adaptation within the Buckingham Canal ecosystem, particularly in response to heavy metal contamination. Enumeration of bacteria from water samples revealed a considerable microbial load, with Sample 1 displaying the highest colony-forming units (3.2×10^5 CFU/mL), indicative of a nutrient-rich and polluted environment that supports microbial proliferation. This high bacterial density correlates well with the observed heavy metal tolerance among the isolates, suggesting long-term environmental pressure selecting for resistant strains. Reports of maximum tolerable concentration (MTC) for various *Bacillus* species commonly fall below 1700–1900 ppm for Pb and other metals in environmental isolates, although values vary by isolate and source. In contrast, BCSS17 combines exceptionally high metal-tolerance with robust sequestration: it tolerates Pb up to 2100 ppm and Cr up to 1900 ppm, and 1700 ppm for both Zn and Mn values that exceed many published environmental isolates. Compared to the findings of Glory's study, which reported that bacterial isolates could resist up to 800 ppm of Co, Cd, and Zn, 400 ppm of Pb, and 100 ppm of Hg, the bacterial isolate BCSS17 from the present study exhibited significantly higher metal toleranceWhile Glory identified *Priestia aryabhattai* and *Enterobacter cloacae* as resistant strains, the superior tolerance displayed by BCSS17 highlights its potential as a highly effective candidate for bioremediation in environments with extreme heavy metal contamination (Ojo et al. 2023).

In Zainab's study, the isolate *B. paramycoides* (strain Z1) exhibited strong resistance to ampicillin (1500 μg/ml) and produced exopolysaccharides (EPS) containing alkenes, alkynes, and carboxylic acids, as confirmed by FTIR (Hassan et al. 2024). In contrast, the *B. paramycoides* isolate from the present study displayed multidrug resistance to cephalothin, ceftizoxime, cefuroxime, amoxiclav, nitrofurantoin, trimethoprim, and tobramycin, while remaining sensitive to

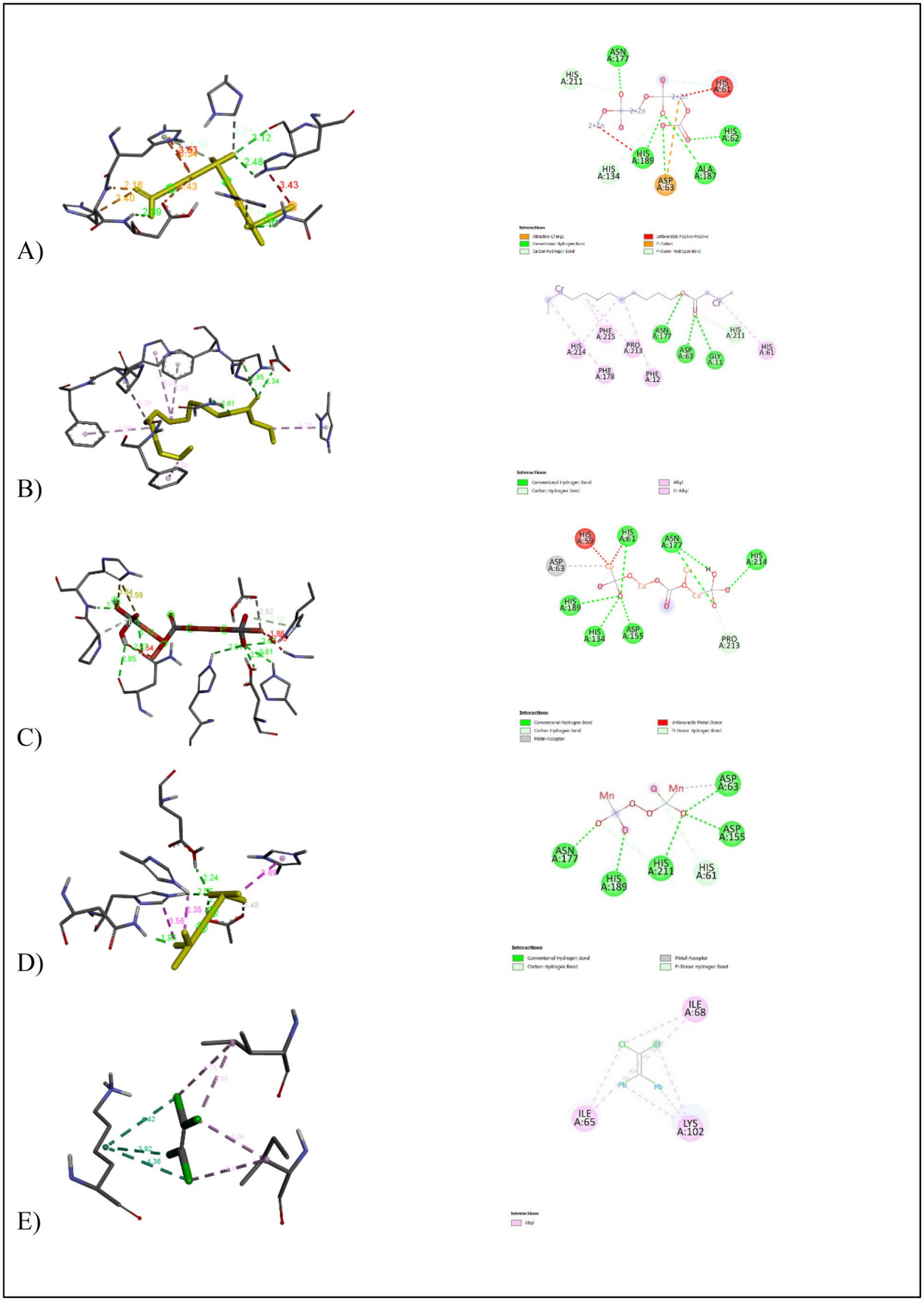

Figure 9. Interaction of metallo beta lactamse with A) Zinc oxide, B) chromium oxide, C) copper oxide, D) Manganese oxide, E) lead chloride.

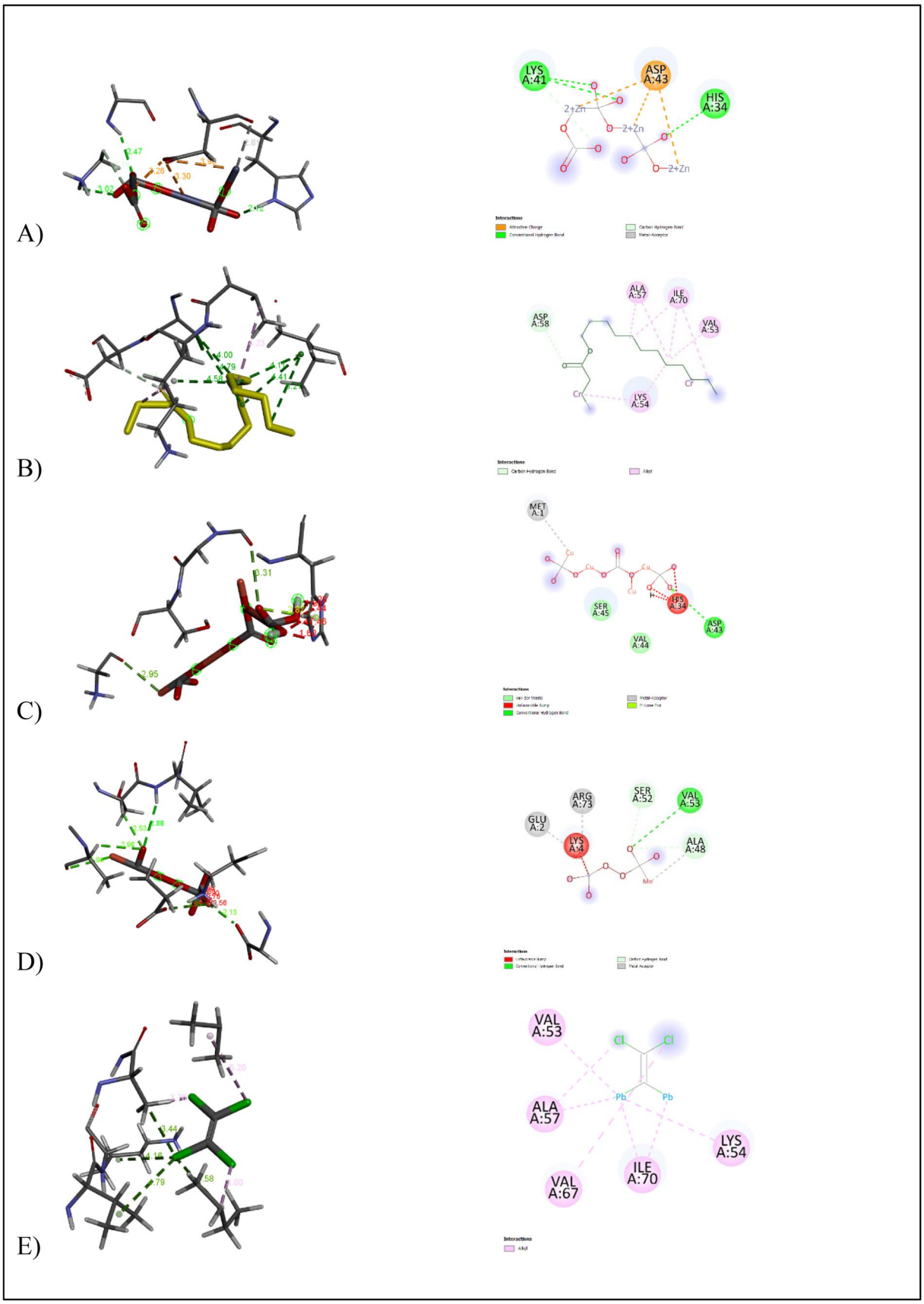

Figure 10. Interaction of metallochaperone with A) Zinc oxide, B) chromium oxide, C) copper oxide, D) Manganese oxide, E) lead chloride.

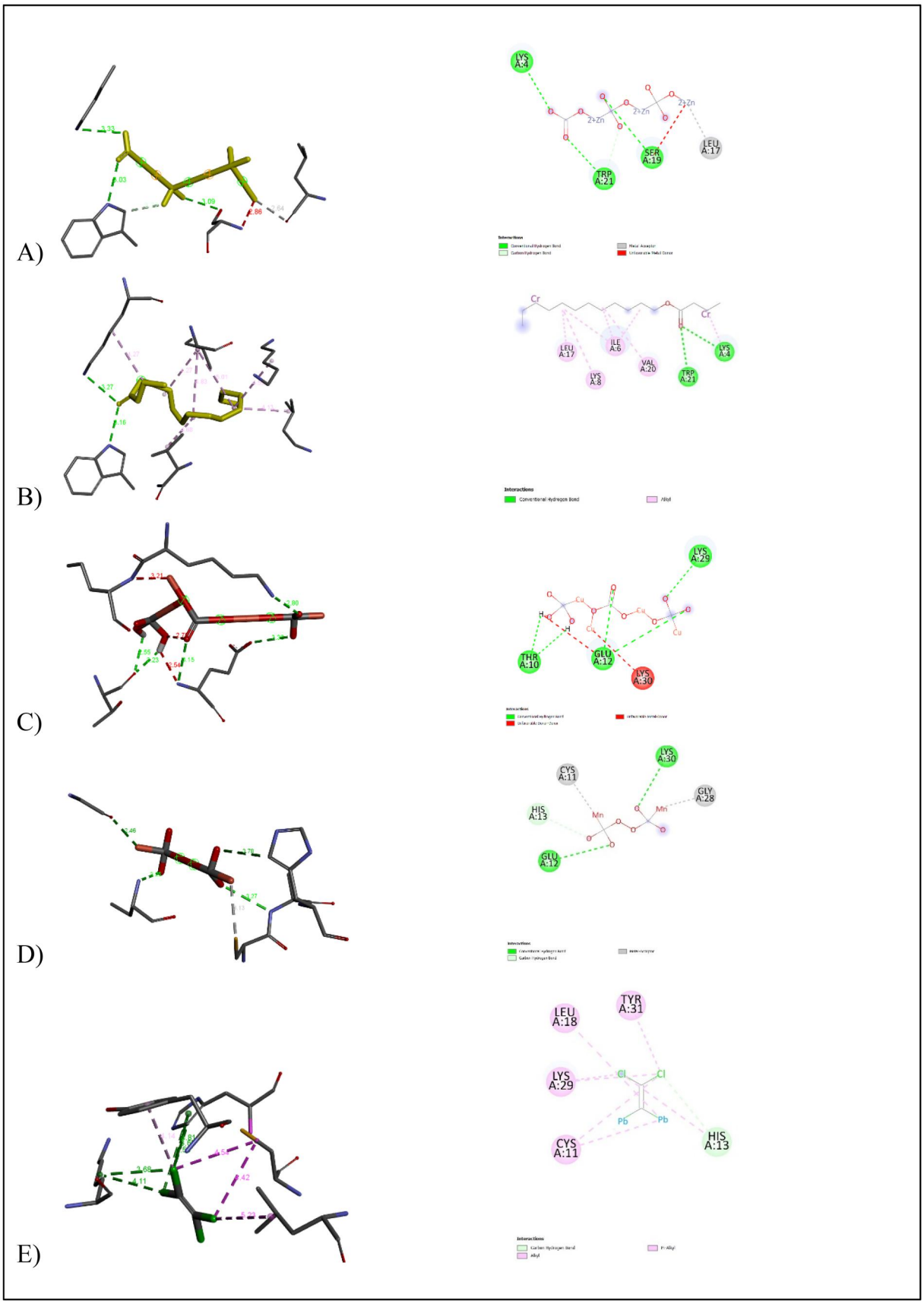

Figure 11. Interaction of metallothionein with A) Zinc oxide, B) chromium oxide, C) copper oxide, D) Manganese oxide, E) lead chloride.

cefotaxime, norfloxacin, ofloxacin, levofloxacin, and amikacin. This broader resistance pattern likely reflects adaptation to combined antibiotic and heavy metal pressures in an aquatic ecosystem. This multi-drug resistance profile suggests a possible co-selection mechanism where exposure to heavy metals may contribute to the maintenance or acquisition of antibiotic resistance genes—a phenomenon often attributed to co-resistance or cross-resistance mechanisms mediated by mobile genetic elements (Kadhim et al. 2024). In Glory's study, molecular analysis revealed the presence of HMRGs such as *merA*, *cnrA*, and *pocC* in *Enterobacter cloacae*, supporting its potential for bioremediation in gold mining sites. In contrast, gene amplification in the present study confirmed that *B. paramycoides* harbors *zntA* and *pbrA*, which are specifically associated with resistance to Zn and Pb (Ojo et al. 2023). This genetic evidence aligns with BCSS17's high MTC values and further underscores its superior adaptability and suitability for bioremediation in environments with complex and high-level heavy metal contamination.

Finally, molecular identification through 16S rRNA sequencing confirmed BCSS17 as *Bacillus paramycoides*, with 100% sequence identity. This species is known for its environmental resilience and metabolic versatility, aligning with the isolate's resistance traits. The integration of physiological, genetic, and phylogenetic data collectively positions *Bacillus paramycoides* as a promising candidate for bioremediation in heavy metal-polluted environments. Collectively, this study not only expands our understanding of microbial ecology in polluted environments but also presents *Bacillus paramycoides* as a novel, high-potential candidate for developing sustainable bioremediation strategies targeting multi-metal contaminated aquatic ecosystems.

The research results from the growth profile, heavy metal uptake, and bioaccumulation assays for *B. paramycoides* exhibit a coherent pattern that emphasizes the bacterium's high tolerance and bioremediation potential, particularly for Pb and Zn. In the growth profile study, the highest OD was recorded in the presence of Pb (1.643 at 25 h), followed by Zn (1.587), indicating substantial tolerance and active proliferation in these metal environments. This robust growth corresponds directly with the uptake results, where Pb demonstrated the highest biosorption capacity (5.024 ± 0.57 mg/g at 100 ppm) and maintained significant uptake even at elevated concentrations. Similarly, Zn uptake peaked at 4.128 ± 0.52 mg/g at 200 ppm, reflecting strong cellular affinity.

The findings of Hanjun's study on *Bacillus* sp. EB L14 and the present investigation on *Bacillus paramycoides* both underscore the genus's potential for heavy metal bioremediation, though notable differences in metal-specific uptake and experimental conditions are evident. Hanjun reported high uptake efficiencies at low metal concentrations (10 mg/L), with 80.48% for Pb, 75.78% for Cd, and a significantly lower 21.25% for Cu, while chromium showed negligible uptake. The study also suggested that inhibiting ATPase activity could enhance remediation efficiency, indicating an energy-dependent metal transport mechanism (Hanjun et al. 2010). In contrast, the current study evaluated *B. paramycoides* over a broader concentration range (100–500 ppm), demonstrating peak Zn accumulation at 73.128 ± 0.62% at 200 ppm and high Pb accumulation up to 69.435 ± 0.33% at 400 ppm, reflecting strong binding capacity even at elevated concentrations (Table 6). Cr exhibited moderate accumulation (47.127–30.367%), unlike the negligible uptake seen in Hanjun's strain EB L14. These differences suggest that *B. paramycoides* possesses a broader tolerance and effective bioaccumulation capacity across a wider concentration range, particularly for Zn and Pb, making it a strong candidate for bioremediation in more heavily contaminated environments. In contrast, Cu and Cr exhibited lower growth support (OD ~1.5 and 1.38, respectively), reduced uptake (<1.0 mg/g at 400 ppm for Cu), and diminished accumulation percentages at higher concentrations, highlighting their greater toxicity and possible interference with metabolic processes

The SEM and FTIR analyses complement and strengthen the findings from the growth profile, metal uptake, and bioaccumulation assays of *B. paramycoides*, providing molecular and morphological evidence for heavy metal interaction and toxicity. SEM images revealed pronounced structural damage under Pb and Cr exposure,

consistent with reduced growth rates and high biosorption levels.

The FTIR results from the present study reveal distinct biochemical interactions between *B. paramycoides* and various heavy metals, highlighting differential stress responses and binding mechanisms, which can be compared with the findings of Zainab's study. Zainab's strain Z1 produced EPS containing functional groups such as alkenes, alkynes, and carboxylic acids, indicating its chemical complexity and potential for metal interaction (Zainab et al. 2024). However, her study did not link specific FTIR peaks to individual metal responses. In contrast, the current study provides a more detailed spectrum-based analysis: Pb exposure induced C=O stretching at 1724.02 cm^{-1} and strong amide band shifts, reflecting intense protein and polysaccharide engagement and severe membrane disintegration.

The Pb caused membrane disintegration, aligning with the FTIR detection of unique peaks like C=O stretching (1724.02 cm^{-1}) and strong shifts in amide bands, indicating intense protein and polysaccharide interaction and cellular stress. Cr similarly disrupted cellular morphology and caused structural deformation, reflected in the FTIR spectrum by peaks like 1451.25 cm^{-1}, indicating cell wall modifications.

Zn-treated cells, which showed enhanced growth and bioaccumulation (peak 73.128% at 200 ppm), exhibited minor morphological damage and moderate FTIR shifts, suggesting biosorption with less structural impact. The interaction involved O–H, amide, and polysaccharide groups without metal–O vibration peaks, implying surface-level binding with minimal toxicity. Mn also triggered moderate structural changes and exhibited FTIR peaks associated with carbonyl, amide, and phosphate groups, aligning with intermediate uptake and bioaccumulation.

FTIR spectra of Cu and Cr treatments showed phosphate and metal–O vibrational disrupted protein structure, correlating with their relatively low uptake and bioaccumulation, as well as reduced growth. These findings suggest that while *Bacillus paramycoides* interacts with all metals *via* functional groups like carboxyl, phosphate, and amines, the extent of binding and resultant toxicity varies. Pb and Zn bind effectively with manageable stress, while Cu and Cr induce more cellular disruption, limiting bioremediation efficiency.

Amani focused on the docking of β-lactam antibiotics (ampicillin, imipenem, nitrocefin, and aztreonam) to the active site of metallo-β-lactamase, showing coordination with Zn^{2+} ions *via* C3/C4-carboxylates and β-lactam oxygen atoms. Key residues such as Asn220 and Lys211 formed hydrogen bonds and salt bridges, while hydrophobic residues (Met67, Phe70, Val73, Trp93) contributed to substrate stabilization. Notably, coordination with Zn1 and Zn2 varied between antibiotics, indicating substrate-specific binding modes (Eshtiwi Amani & Rathbone, 2023).

In contrast, the present study evaluated the interaction of heavy metal oxides (ZnO, $PbCl_2$, Cr_2O_3, CuO, MnO) with metallo-β-lactamase, metallochaperone, and metallothionein in *Bacillus paramycoides*. For metallo-β-lactamase, ZnO exhibited the strongest binding energy (–9.6 kcal/mol), with interactions dominated by histidine residues (HIS A:61, A:62, A:134, A:189, A:211) and acidic residues (ASP A:63, ASN A:177), forming a coordination network similar in role to Amani's Zn-ligating residues. The $PbCl_2$ also formed a highly stable complex (–8.6 kcal/mol), primarily *via* HIS A:61, A:189, A:211, ASP A:63, and A:155, resembling the strong electrostatic and chelating interactions observed in Amani's antibiotic docking but in the context of metal detoxification. Furthermore, while Amani identified His250 as a unique Zn-coordinating residue with hydrophobic contacts, the current study showed broad involvement of histidines and aspartates in metal binding across all proteins, extending beyond a single zinc ion and encompassing multiple metal types. The binding patterns reflect broader metal affinity (biosorption) rather than enzymatic inhibition. Compared to the study of Sugitha et al. (2025) of *Proteus mirabilis*, *Bacillus paramycoides* demonstrates a markedly stronger and broader heavy-metal binding capability, making it the more effective candidate for bioremediation. *P. mirabilis* displayed more protein-specific binding, with metallothionein SmtA showing the highest ZnO affinity across both species (–9.8 kcal/mol), dominated by acidic and aromatic residues that favor Zn and Mn

chelation, and its metal affinity is more protein-specific and narrower in scope (Sugitha et al. 2025). Overall, *Bacillus paramycoides* outperforms *Proteus* in handling a wider range of heavy metals, especially lead, underscoring its superior potential for bioremediation applications.

The interaction between metallo β-lactamase and lead reveals a compact and highly stable coordination network, with active site residues positioned at precise distances conducive to strong metal binding. The Pb ion is centrally located and coordinated by key residues including HIS A:61, HIS A:189, HIS A:211, ASP A:63, ASP A:155, and ASN A:177 (Table 8). Among these, the aspartate residues (ASP A:63 and ASP A:155) form the shortest and strongest interactions, with bond distances of approximately 1.91–1.92 Å, indicating robust electrostatic attraction and chelation *via* their negatively charged carboxylate groups. The histidine residues, known for their metal-chelating imidazole nitrogen atoms, contribute significantly as well—HIS A:61, HIS A:189, and HIS A:211 show coordination distances ranging from 2.04 to 2.36 Å, suggesting strong coordinate bonding. Additionally, ASN A:177 participates *via* its amide group, maintaining a slightly longer interaction distance of around 2.42 Å, likely contributing to the stability of the metal complex through weaker hydrogen bonding or coordination. These precise residue-metal distances reflect an optimized binding geometry that supports the observed high binding affinity (–8.6 kcal/mol), confirming the enzyme's potential role in lead detoxification and bioremediation.

The ZnO also showed strong binding with Metallothionein (−8.8 kcal/mol) and moderate binding with Metallochaperone (−8.3 kcal/mol). The 3D docking images show hydrogen bonds and metal coordination distances, indicating spatial compatibility and binding intensity (Figures 9, 10, and 11). The Cr_2O_3 consistently showed the weakest binding across all proteins, particularly Metallo-β-lactamase (−4.3 kcal/mol), suggesting lower biosorption potential. However, unique residue involvement (e.g., CH_2 deformations from FTIR and distinct PHE and GLY residues) indicates different coordination modes.

This research presents a novel and comprehensive evaluation of *Bacillus paramycoides* BCSS17, highlighting its exceptional bioremediation potential against multiple heavy metals—particularly Pb and Zn, through a multidisciplinary approach integrating microbiological, biochemical, molecular, and computational analyses. Unlike previous studies that often focus solely on metal tolerance or biosorption capabilities, this work uniquely combines MTC assays, growth kinetics, uptake and bioaccumulation profiling, SEM and FTIR characterization, gene amplification, and molecular docking, offering an in-depth mechanistic understanding of metal interaction at both cellular and protein levels. Notably, the co-occurrence of heavy metal and antibiotic resistance, supported by the presence of *zntA* and *pbrA* genes, underscores the dual adaptive traits of the isolate. Molecular docking revealed precise metal–protein interactions with key residues, elucidating potential enzymatic roles in metal sequestration. This integrated methodology and identification of *B. paramycoides* as a potent multi-metal bioremediator mark a significant advancement over prior works, which often overlook molecular confirmation of biosorptive function and structural integrity under metal stress.

Conclusion

This study comprehensively characterizes *Bacillus paramycoides*, isolated from the heavily polluted Buckingham Canal, as a highly tolerant and efficient biosorbent for heavy metals, especially lead and zinc. The isolate demonstrated exceptional multi-metal resistance, corroborated by high MTC values, biosorption, and bioaccumulation efficiencies. Molecular analyses revealed the presence of *zntA* and *pbrA* genes, linking genotypic resistance to phenotypic traits. Advanced SEM and FTIR studies provided mechanistic insights into metal-induced structural alterations and functional group involvement, while molecular docking further validated protein–metal interactions, with strong binding affinities observed for Pb and Zn with Metallo-β-lactamase and Metallothionein. Unlike earlier studies that often lack molecular correlation, this research integrates microbial physiology, spectroscopy, and computational modeling, thereby offering a novel, multi-tiered approach to evaluating

bioremediation potential. *B. paramycoides* BCSS17 emerges as a promising candidate for eco-friendly remediation of multi-metal contaminated aquatic ecosystems, paving the way for sustainable environmental management strategies grounded in microbial biotechnology.

Acknowledgements

We are grateful to Vels Institute of Science, Technology and Advanced Studies (VISTAS) for generously providing the facilities and space to conduct our research.

Data availability statement

The data supporting the findings of this study are available from the corresponding author upon reasonable request.

Authors' contributions

S.S. and G.A. jointly conceptualized and designed the study. **S.S.** conducted the experiments, collected the data, and performed the initial analysis. **M.S. and K.A.** carried out the critical review and editing. **M.J.** revised the manuscript. **G.A.** contributed to data interpretation, statistical analysis, and manuscript preparation. All authors participated in drafting and revising the manuscript and approved the final version for submission.

Disclosure statement

No potential conflict of interest was reported by the author(s).

Consent for publication

All authors agree to publish the following manuscript

References

Ahmed I, Zakiya A, Fazio F. 2022. Effects of aquatic heavy metal intoxication on the level of hematocrit and hemoglobin in fishes: a review. Front Environ Sci. 10:132 https://doi.org/10.3389/fenvs.2022.919204

Ali H, Khan E. 2019. Trophic transfer, bioaccumulation, and biomagnification of non-essential hazardous heavy metals and metalloids in food chains/webs—Concepts and implications for wildlife and human health. Human and Ecol Risk Assess. 25(6):1353–1376. https://doi.org/10.1080/10807039.2018.1469398

Anwar M, Ali S, Asaad A. 2017. Evaluation of heavy metals resistant *Micrococcus sp.* Isolated from rivers in Basra, Iraq. J Bioremediat Biodegrad. 8(1):1–4. https://doi.org/10.4172/2155-6199.1000383

Ayodele PF et al. 2023. Illustrated procedure to perform molecular docking using pyrx and biovia discovery studio visualizer: a case study of 10kt with atropine. Prog Drug Discov Biomed Sci. 6(1):1–32. https://doi.org/10.36877/pddbs.a0000424

Banaee M, Zeidi A, Mikušková N, Faggio C. 2024. Assessing metal toxicity on crustaceans in aquatic ecosystems: a comprehensive review. Biol Trace Elem Res. 202(12):5743–5761. https://doi.org/10.1007/s12011-024-04122-7

Benmalek Y, Fardeau M. 2016. Isolation and characterization of metal-resistant bacterial strain from wastewater and evaluation of its capacity in metal-ions removal using living and dry bacterial cells. Int J Environ Sci Technol. 13(9):2153–2162. https://doi.org/10.1007/s13762-016-1048-6

Bergey DH, Holt JG. 2000. Bergey's manual of determinative bacteriology. 9th ed. Baltimore (MD): Williams & Wilkins. 787 pp.

Berkman SJ, Roscoe EM, Bourret JC. 2019. Comparing self-directed methods for training staff to create graphs using Graphpad Prism. J Appl Behav Anal. 52(1):188–204. https://doi.org/10.1002/jaba.522

Burley SK et al. 2021. RCSB Protein Data Bank: powerful new tools for exploring 3D structures of biological macromolecules for basic and applied research and education in fundamental biology, biomedicine, biotechnology, bioengineering and energy sciences. Nucleic Acids Res. 49(D1):D437–D451. https://doi.org/10.1093/nar/gkaa1038

Chaudhari R, Li Z. 2015. PyMine: a PyMOL plugin to integrate and visualize data for drug discovery. BMC Res Notes. 8(1):517. https://doi.org/10.1186/s13104-015-1483-3

Deng M-H, Li K, Yan Y, Huang F, Peng D. 2022. Enhanced cadmium removal by growing Bacillus cereus RC-1 immobilized on different magnetic biochars through simultaneous adsorption and bioaccumulation. Environ Sci Pollut Res Int. 29(13):18495–18507. https://doi.org/10.1007/s11356-021-17125-x

Dinku A, Jiru TM. 2025. Isolation, screening, and characterization of heavy metal-resistant bacteria from solid waste dumping sites in Central Gondar, Northwest, Ethiopia. Sci Prog. 108(1):368504251315807. https://doi.org/10.1177/00368504251315807

Eberhardt J, Santos-Martins D, Tillack AF, Forli S. 2021. AutoDock Vina 1.2.0: new docking methods, expanded force field, and python bindings. J Chem Inf Model. 61(8):3891–3898. https://doi.org/10.1021/acs.jcim.1c00203

El Khoury G, Azzam W, Rebehmed J. 2023. PyProtif: a PyMol plugin to retrieve and visualize protein motifs for structural studies. Amino Acids. 55(10):1429–1436. https://doi.org/10.1007/s00726-023-03323-z

Eshtiwi AA, Rathbone DL. 2023. A modified bonded model approach for molecular dynamics simulations of New Delhi Metallo-β-lactamase. J Mol Graph Model. 121:108431. https://doi.org/10.1016/j.jmgm.2023.108431

Ghafarifarsani H et al. 2024. Pesticides and heavy metal toxicity in fish and possible remediation – a review. Ann

Animal Sci. 24(4):1007–1024. https://doi.org/10.2478/aoas-2024-0012

Häder D-P et al. 2020. Anthropogenic pollution of aquatic ecosystems: emerging problems with global implications. Sci Total Environ. 713:136586. https://doi.org/10.1016/j.scitotenv.2020.136586

Hanjun G et al. 2010. Bioremediation of heavy metals by growing hyperaccumulaor endophytic bacterium *Bacillus sp*. L14. Bioresour Technol. 101(22):8599–8605. https://doi.org/10.1016/j.biortech.2010.06.085

Hassan Z, Jamil N, Batool R. 2024. Exploring antibiotic resistance and exopolysaccharide production in *Bacillus paramycoides* from wastewater. J Bioresource Manage. 6: 212–224.

Hnatush S et al. 2020. Morphological, physiological and biochemical properties of heavy metal resistant isolates of bacteria obtained from different Antarctic substrates. Ukrainian Antarctic J. 1:82–92. https://doi.org/10.33275/1727-7485.1.2020.381

Huang J, Liu C, Price GW, Li Y, Wang Y. 2021. Identification of a novel heavy metal resistant *Ralstonia* strain and its growth response to cadmium exposure. J Hazard Mater. 416:125942. https://doi.org/10.1016/j.jhazmat.2021.125942

Humphries R, Bobenchik A, Hindler J, Schuetz A. 2021. Overview of changes to the clinical and laboratory standards institute performance standards for antimicrobial susceptibility testing, M100, 31st Edition. J Clin Microbiol. 59(12):e00213-21. https://doi.org/10.1128/JCM.00213-21

Ibrahim L, Rashed RO, Muhammed S. 2021. Evaluation of heavy metal content in water and removal of metals using native isolated bacterial strains. Biodiversitas. 22(8): 3163–3174. https://doi.org/10.13057/biodiv/d220810

Jeong H, Byeon E, Kim D-H, Maszczyk P, Lee J-S. 2023. Heavy metals and metalloid in aquatic invertebrates: a review of single/mixed forms, combination with other pollutants, and environmental factors. Mar Pollut Bull. 191: 114959. https://doi.org/10.1016/j.marpolbul.2023.114959

Kadhim AA, Mohammed M, Jabbar AD. 2024. Role of heavy metals pollution on emergence of antibiotic co-resistance in E. coli isolates. Adv Life Sci. 11(4):887. https://doi.org/10.62940/als.v11i4.3352

Kassim A, Omuse G, Premji Z, Revathi G. 2016. Comparison of clinical laboratory standards institute and european committee on antimicrobial susceptibility testing guidelines for the interpretation of antibiotic susceptibility at a university teaching hospital in nairobi, kenya: a cross-sectional study. Ann Clin Microbiol Antimicrob. 15(1):21. https://doi.org/10.1186/s12941-016-0135-3

Khalifa AM et al. 2025. Geospatial assessment of heavy metal contamination and metal-resistant bacteria in Qarun Lake, Egypt. Environ Sci Eur. 37(1):106. https://doi.org/10.1186/s12302-025-01152-3

Khan MSI, Oh S-W, Kim Y-J. 2020. Power of scanning electron microscopy and energy dispersive x-ray analysis in rapid microbial detection and identification at the single cell level. Sci Rep. 10(1):2368. https://doi.org/10.1038/s41598-020-59448-8

Kim S et al. 2007. Characterisation of heavy metal tolerance and biosorption capacity of bacterium strain CPB4 (*Bacillus spp*.). Water Sci Technol. 55(1–2):105–111. https://doi.org/10.2166/WST.2007.007

Kim S et al. 2016. PubChem substance and compound databases. Nucleic Acids Res. 44(D1):D1202–D1213. https://doi.org/10.1093/nar/gkv951

Kim S et al. 2023. PubChem 2023 update. Nucleic Acids Res. 51(D1):D1373–D1380. https://doi.org/10.1093/nar/gkac956

Kuma SV, Pascal LF, Meeran M. 2020. Comprehensive analysis on the physical, chemical, nutrient, heavy metal and microbiological parameters at selected stations of Buckingham Canal,Chennai, Tamil Nadu, India. Environmental Contaminants Rev (ECR) 3(2):77–86.

Kumar M et al. 2024. A review on heavy metal-induced toxicity in fishes: bioaccumulation, antioxidant defense system, histopathological manifestations, and transcriptional profiling of genes. J Trace Elem Med Biol. 83:127377. https://doi.org/10.1016/j.jtemb.2023.127377

Kumar S, Sultana M, Pascal L. 2018. Analysis of a few heavy metals in Buckingham Canal water. IJZS. 3(1):232–235.

Kumar SV, Tennyson S, Sultana M, Pasca LF. 2018. Analysis of physicochemical water quality parameters of Buckingham Canal. IJZS. 3(1):226–231.

Li X, Li D, Yan Z, Ao Y. 2018. Biosorption and bioaccumulation characteristics of cadmium by plant growth-promoting rhizobacteria. RSC Adv. 8(54):30902–30911. https://doi.org/10.1039/C8RA06270F

Mitra M, Nguyen KM-A-K, Box TW, Berry TL, Fujita M. 2021. Isolation and characterization of a heavy metal- and antibiotic-tolerant novel bacterial strain from a contaminated culture plate of *Chlamydomonas reinhardtii*, a green micro-alga. F1000Res. 10:533. https://doi.org/10.12688/f1000research.53779.2

Muhammed A, Abbas A. 2021. Molecular detection of some heavy metal resistance genes in lead resistant bacteria. Adv Life Sci. 3(2):87.

Nandiyanto ABD, Oktiani R, Ragadhita R. 2019. How to read and interpret FTIR spectroscope of organic material. Indonesian J Sci Technol. 4(1):97. https://doi.org/10.17509/ijost.v4i1.15806

Ojo GJ et al. 2023. Physiochemical analyses and molecular characterization of heavy metal-resistant bacteria from Ilesha gold mining sites in Nigeria. J Genet Eng Biotechnol. 21(1):172. https://doi.org/10.1186/s43141-023-00607-5

Podder M, Majumder C. 2017. Simultaneous biosorption and bioaccumulation: a novel technique for the efficient removal of arsenic. Sustain Water Resour Manag. 3(4): 357–389. https://doi.org/10.1007/s40899-017-0103-x

Prashanthi R, Shreevatsa GK, Krupalini S, Manoj L. 2021. Isolation, characterization, and molecular identification of soil bacteria showing antibacterial activity against human

pathogenic bacteria. J Genet Eng Biotechnol. 19(1):120. https://doi.org/10.1186/s43141-021-00219-x

Roux C et al. 2024. Impact of urban pollution on freshwater biofilms: oxidative stress, photosynthesis and lipid responses. J Hazard Mater. 472:134523. https://doi.org/10.1016/j.jhazmat.2024.134523

Santhosh K et al. 2024. Unveiling the silent threat: heavy metal toxicity devastating impact on aquatic organisms and DNA damage. Mar Pollut Bull. 200:116139. https://doi.org/10.1016/j.marpolbul.2024.116139

Saqib S et al. 2025. Identifying hotspots and climate drivers of alien plant species for conservation prioritization across the Pan-Himalaya. Biol Conserv. 302:110994. https://doi.org/10.1016/j.biocon.2025.110994

Satapute P, Paidi MK, Kurjogi M, Jogaiah S. 2019. Physiological adaptation and spectral annotation of Arsenic and Cadmium heavy metal-resistant and susceptible strain *Pseudomonas taiwanensis*. Environ Pollut. 251:555–563. https://doi.org/10.1016/j.envpol.2019.05.054

Sayers E et al. 2022. Database resources of the national center for biotechnology information. Nucleic Acids Res. 50(D1):D20–D26. https://doi.org/10.1093/nar/gkab1112

Sayers E et al. 2024. GenBank 2024 update. Nucleic Acids Res. 52(D1):D134–D137. https://doi.org/10.1093/nar/gkad903

Sedlakova-Kadukova J, Kopcakova A, Gresakova L, Godany A, Pristas P. 2019. Bioaccumulation and biosorption of zinc by a novel Streptomyces K11 strain isolated from highly alkaline aluminium brown mud disposal site. Ecotoxicol Environ Saf. 167:204–211. https://doi.org/10.1016/j.ecoenv.2018.09.123

Seeliger D, de Groot BL. 2010. Ligand docking and binding site analysis with PyMOL and Autodock/Vina. J Comput Aided Mol Des. 24(5):417–422. https://doi.org/10.1007/s10822-010-9352-6

Sehnal D et al. 2021. Mol* Viewer: modern web app for 3D visualization and analysis of large biomolecular structures. Nucleic Acids Res. 49(W1):W431–W437. https://doi.org/10.1093/nar/gkab314

Sendolo D, Baysah G, Ezeamagu CO. 2022. Detection of heavy metal-resistance gene in bacteria isolated from clinical and environmental sources using polymerase chain reaction (pcr). AJHES. 1(2):83–92. https://doi.org/10.56893/ajhes.2022-v1i2.239

Sevgi E, Coral G, Gizir A, Sangün M. 2010. Investigation of heavy metal resistance in some bacterial strains isolated from industrial soils. Turkish J Biol. 34:423–431. https://doi.org/10.3906/biy-0901-23

Shahjahan M et al. 2022. Effects of heavy metals on fish physiology - A review. Chemosphere. 300:134519. https://doi.org/10.1016/j.chemosphere.2022.134519

Sharma M, Kant R, Sharma A, Sharma A. 2025. Exploring the impact of heavy metals toxicity in the aquatic ecosystem. Int J Energ Water Res. 9(1):267–280. https://doi.org/10.1007/s42108-024-00284-1

Sheng X-F, Xia J-J, Jiang C-Y, He L-Y, Qian M. 2008. Characterization of heavy metal-resistant endophytic bacteria from rape (*Brassica napus*) roots and their potential in promoting the growth and lead accumulation of rape. Environ Pollut. 156(3):1164–1170. https://doi.org/10.1016/j.envpol.2008.04.007

Sugitha S et al. 2025. Mycoremediation of heavy metals by *Curvularia lunata* from Buckingham Canal, Neelankarai, Chennai. World J Microbiol Biotechnol. 41(1):1. https://doi.org/10.1007/s11274-024-04218-1

Sugitha S, Abirami G. 2025. Heavy metal pollution assessment and bioremediation potential of multidrug-resistant *Proteus mirabilis* isolated from Buckingham canal, Chennai. Biodegradation. 36(4):63. https://doi.org/10.1007/s10532-025-10163-z

Titze B, Genoud C. 2016. Volume scanning electron microscopy for imaging biological ultrastructure. Biol Cell. 108(11):307–323. https://doi.org/10.1111/boc.201600024

Trott O, Olson AJ. 2010. AutoDock Vina: improving the speed and accuracy of docking with a new scoring function, efficient optimization, and multithreading. J Comput Chem. 31(2):455–461. https://doi.org/10.1002/jcc.21334

Ullah A, Hazrat A, Khan BA, Saqib S, Ullah F. 2025. Mitigating lead stress in barley using gibberellic acid (GA3): effects on morpho-physiological and biochemical parameters. J Plant Growth Regul. 44(7):3853–3864. https://doi.org/10.1007/s00344-025-11654-2

Ullah F et al. 2025. Toxicological complexity of microplastics in terrestrial ecosystems. iScience. 28(2):111879. https://doi.org/10.1016/j.isci.2025.111879

Wang J. 2022. A review on the ecotoxicological effects of heavy metals on aquatic organisms-siftdesk. SDRP J Earth Sciences & Environ Stud. 6(2):148. https://doi.org/10.25177/jeses.6.2.ra.10797

Wang Y et al. 2010. An overview of the PubChem BioAssay resource. Nucleic Acids Res. 38(Database issue):D255–D266. https://doi.org/10.1093/nar/gkp965

Wnorowski A. 1991. Selection of bacterial and fungal strains for bioaccumulation of heavy metals from aqueous solutions. Water Sci Technol. 23(1–3):309–318. https://doi.org/10.2166/wst.1991.0429

Yang S et al. 2020. Presence of heavy metal resistance genes in *Escherichia coli* and *Salmonella,* and analysis of resistance gene structure in *E. Coli* e308. J Glob Antimicrob Resist. 21:420–426. https://doi.org/10.1016/j.jgar.2020.01.009

Yushin N et al. 2022. Biosorption and bioaccumulation capacity of arthrospira platensis toward yttrium ions. Metals (Basel). 12(9):1465. https://doi.org/10.3390/met12091465

Zhang H, Zhao Y, Wang Z, Liu Y. 2021. Distribution characteristics, bioaccumulation and trophic transfer of heavy metals in the food web of grassland ecosystems. Chemosphere. 278:130407. https://doi.org/10.1016/j.chemosphere.2021.130407